Direct Photodesorption of Atomic Hydrogen from Si(100) at 157 nm: Experiment and Simulation

T. Vondrak and X.-Y. Zhu*

Department of Chemistry, University of Minnesota, Minneapolis, Minnesota 55455

Received: February 23, 1999; In Final Form: April 22, 1999

Atomic hydrogen photodesorbs from the Si(100)−(2 × 1):H monohydride surface at 157 nm, with a cross section of $\sim 3 \times 10^{-21}$ cm^2. We determine using polarized light that the transition dipole moment for the optical excitation is oriented at ∼18° from the surface normal, as expected for the $\sigma \rightarrow \sigma^*$ transition within the H−Si bond. This result unambiguously establishes the dissociation of the H−Si surface bond by direct optical excitation. The dynamics of this process is characterized by a translational energy of $\langle E_{trans} \rangle = 0.24 \pm 0.02$ eV for atomic H and an isotope effect in photodesorption yield of $y_H/y_D = 10 \pm 3$. We carry out time-dependent quantum mechanical simulation on ab initio potential energy surfaces. The simulation suggests a subfemtosecond lifetime in the excited state and a quantum yield for atomic hydrogen desorption of the order 10^{-5}. This study provides an extreme example for bond-selective photochemistry in large chemical systems. In addition to its significance in understanding ultrafast surface dynamic processes, the direct photodesorption process demonstrated here may also find applications as resistless photolithography in semiconductor technology.

1. Introduction

Due to the presence of extremely efficient energy relaxation pathways on solid surfaces, direct photodissociation of an adsorbate−surface bond is perhaps the most difficult form of bond-selective photochemistry in large chemical systems. Early studies considered direct infrared (IR) photoexcitation of the vibrational ladder in the adsorbate−surface potential well.[1,2] However, ladder "climbing" by sequential single-photon transitions to reach the desorption continuum is impossible to accomplish with a monochromatic IR laser as a result of anharmonicity, while dipole-forbidden, multilevel "jumping" requires intense laser fields and is not feasible due to surface heating. In most cases, resonant IR photodesorption can be attributed to the excitation of an intramolecular vibrational mode, followed by energy transfer to the substrate or to the adsorbate−surface bond.[3−5] Only for a very weak physisorption well which supports few vibrational levels can direct IR photodesorption become possible.[6]

An alternative to IR photodesorption is the direct photodissociation of an adsorbate−surface bond via valence electronic transitions. This is difficult to realize because the adsorbate−surface bond is viewed as part of a delocalized surface electronic structure and relaxation of electronic excitation energy on surfaces is extremely efficient.[7] Nearly all photodesorption studies point to indirect mechanisms, e.g., those due to hot substrate carriers or to the transfer of intramolecular excitation to the desorption coordinate.[8−10] The best example for the latter is the vibrationally mediated UV photodesorption mechanism for ammonia from semiconductor and metal surfaces, as discovered by Zhu et al.[11−13] and explored by a number of other groups.[14−17] Recently, Matsumoto and co-workers reported that the photochemistry, including desorption and dissociation, of methane weakly adsorbed on Pt(111) resulted from adsorbate-localized optical excitation.[18] However, photodesorption in this case is likely due to intramolecular excitation rather than direct excitation of the adsorbate−surface bond.

The present study is aimed at establishing the direct photodissociation of an adsorbate−surface bond by optical excitation in a model system, Si(100)−(2 × 1):H. This surface is chosen for the following reasons. (i) Previous spectroscopic studies revealed a fairly localized electronic transition at ∼8 eV, which can be assigned to the H−Si $\sigma \rightarrow \sigma^*$ transition.[19,20] (ii) Recent scanning tunneling microscopy (STM) studies showed that hydrogen can be desorbed from Si(100)−(2 × 1):H by the STM tip.[21] The desorption mechanism at a bias voltage higher than 6 eV was interpreted as the excitation of the $\sigma \rightarrow \sigma^*$ transition by field-emitted electrons. The above studies point to the feasibility of dissociating the Si−H bond via direct optical excitation. Indeed, photodesorption of hydrogen-containing species from silicon surfaces was observed in synchrotron radiation assisted epitaxial growth of Si.[22] More recently, Pusel et al. showed a nonthermal origin for H_2 desorption when the Si(111):H surface is irradiated by 7.9 eV photons.[23]

We show that atomic hydrogen photodesorbs from the Si(100)−(2 × 1):H monohydride surface under 157 nm laser irradiation. The transition dipole moment is oriented along the H−Si bond direction. This result unambiguously establishes the direct photodesorption mechanism. A comparison of experiment with time-dependent quantum mechanical simulation suggests an excited-state lifetime of ∼0.4 fs. The example presented demonstrates that optical excitation of valence electronic states on semiconductor surfaces may be viewed on a localized scale, albeit within an ultrashort time window. A brief report of this work has already been published elsewhere.[24]

2. Experimental Section

All experiments were performed in an ultrahigh vacuum (UHV) chamber pumped by a turbo molecular pump with a

* To whom correspondence should be addressed. Phone: (612) 624-7849. Fax: (612) 626-7541. E-mail: zhu@chem.umn.edu.

10.1021/jp990636g CCC: $18.00
Published on Web 05/22/1999

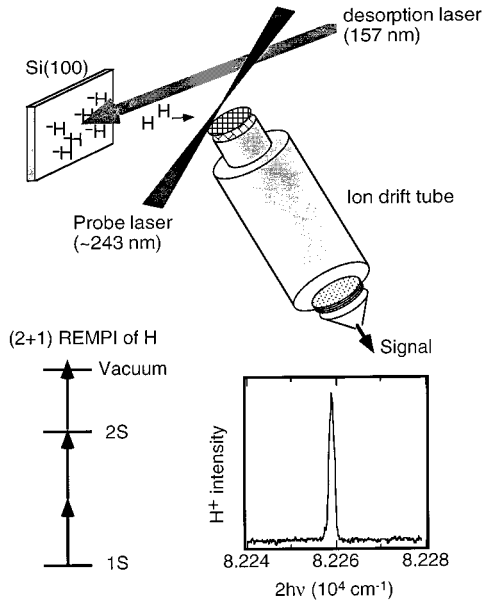

Figure 1. (Upper) experimental setup; (lower left) the (2 + 1) REMPI scheme for atomic hydrogen detection; (lower right) (2 + 1) REMPI spectrum of atomic hydrogen.

base pressure of 1×10^{-10} Torr. The system consisted of two levels. The upper level was equipped with a low-energy electron diffraction (LEED) and Auger electron spectrometer (AES) for surface analysis. The lower level featured a quadrupole mass spectrometer (QMS) and a time-of-flight mass spectrometer (TOFMS). The QMS was used for residual gas analysis (RGA) and thermal desorption spectroscopy (TDS). The TOFMS, equipped with Chevron multichannel plates (MCP) and an impedance-matched fast timing anode, was used for mass-resolved ion detection in resonance-enhanced multiphoton ionization (REMPI) spectroscopy.

The Si(100) sample was a slice ($18 \times 10 \times 0.4$ mm) of an n-type wafer (0.01 Ω cm, Wafernet). After thorough degreasing, we mounted the sample on a sample manipulator using two Ta clips following the procedure described by Yates and co-workers.[25] A type C thermocouple was attached to the sample via a small Ta clip for temperature measurement. The sample was cooled by liquid nitrogen and heated resistively. After system bake out, the sample was first degassed overnight in UHV at 900 K, followed by desorbing the native oxide layer in UHV environment to ~1300−1400 K. Atomic hydrogen (or deuterium) was generated by dissociating H_2 on a hot tungsten filament and dosed onto the clean Si(100) surface. The monohydride Si(100)−(2 × 1):H surface was prepared by a saturation exposure to H at a surface temperature of 600 K.[26] Surface coverage was confirmed by thermal desorption spectroscopy (TDS) which showed a well-characterized peak due to recombinative H_2 desorption from surface monohydride.[27] All experiments reported here employed the monohydride Si(100)−(2 × 1):H surface.

The experimental setup for atomic hydrogen desorption and detection is shown schematically in Figure 1. The photodesorption laser light at 157 nm ($h\nu = 7.9$ eV) was from an excimer laser (LamdaPhysik) filled with a F_2−He mixture. The laser outputs 10 mJ pulse energy at 25 ns pulse width, and it can be operated at repetition rates of 20 Hz or less. A 1 mm^2 portion at the center of the rectangularly shaped laser beam (20 × 7 mm) was selected by an iris and directed into the UHV chamber through a CaF_2 window. In all experiments, the angle of incidence was either 0° or 30° from the surface normal. The reflected light exited the chamber through either the entrance window or a second window. Polarized light was obtained by passing the excimer laser output through a MgF_2 prism polarizer (Optics-For-Research). The laser pulse energy density on the surface was 2 mJ/cm^2 for unpolarized light and 0.5 mJ/cm^2 for polarized light. In all photodesorption experiments presented below, surface temperature was controlled at 420 K.

The probe laser light for the resonance-enhanced multiphoton ionization (REMPI) detection of atomic hydrogen was from an YAG-pumped dye laser (Continuum). The dye output at ~486 nm was frequency doubled in an angle-tuned BBO crystal to generate probe UV light at ~243 nm (1 mJ pulse energy). It was focused by a quartz lens ($f = 25$ cm) and directed into the UHV chamber through a fused silica window. The focal point of the probe laser was located at 17 mm away from the Si sample. H^+ ions in the laser focal volume were extracted into the TOF spectrometer and, after passing through a 30 cm ion drift tube, detected by multichannel plates. The experiment was controlled by LabView-based software on a personal computer equipped with a timing input/output board and a data acquisition board. Both the excimer laser and the YAG laser were triggered at 10 Hz. The time delays were completely software controlled.

The detection of H was achieved via the $2^2S_{1/2} \leftarrow 1^2S_{1/2}$ transition using a two-photon resonance,[28] three-photon ionization scheme, i.e., (2 + 1) REMPI, shown schematically in the lower left part of Figure 1. A typical spectrum is shown in the lower right part. This detection scheme is extremely sensitive and can detect atomic H generated by any filament in the UHV chamber at a base pressure of 1×10^{-10} Torr. To avoid background signal, we turned off all filaments during photodesorption measurement. In experiments presented below, the dye laser was tuned to the peak position and, except for time-of-flight (TOF) measurements, the time delay between the desorption and probe laser pulses was set at the peak TOF position.

Extreme caution has to be taken in carrying out the experiment. The VUV laser light at 157 nm could desorb hydrogen-containing species, including atomic H, from the chamber wall or other surfaces in the UHV environment. We used a small size (1 mm^2) laser beam which irradiated only the center of the Si(100) sample. Careful alignment was necessary to avoid any scattered light on chamber walls or sample manipulators. A small amount of 157 nm light back-reflected from the inner surface of the exit window also terminated at the Si surface. We carried out extensive background experiments using clean Si(100) surfaces to guarantee that atomic H signal from sources other than the Si(100)−(2 × 1):H surface was negligible.

3. Results and Discussion

We organize the Results and Discussion into four sections. In 3.1, we present experimental measurement on the photodesorption cross section for atomic H from Si(100)−(2 × 1):H at 157 nm and show, using polarized light, that photodesorption is due to direct optical excitation of the H−Si surface bond. In 3.2, we present time-of-flight (TOF) distribution of atomic H and the isotope effect in photodesorption cross section. In 3.3, we address the dynamics of this process using time-dependent quantum mechanical simulation and compare computational results with experimental observations. Finally, in section 3.4, we briefly discuss the possible application of this direct photodesorption mechanism in semiconductor technology.

3.1. Probing the Direct Photoexcitation Mechanism by Polarized Light. Irradiating the monohydride Si(100)−(2 × 1):H surface by 157 nm light leads to the desorption of atomic

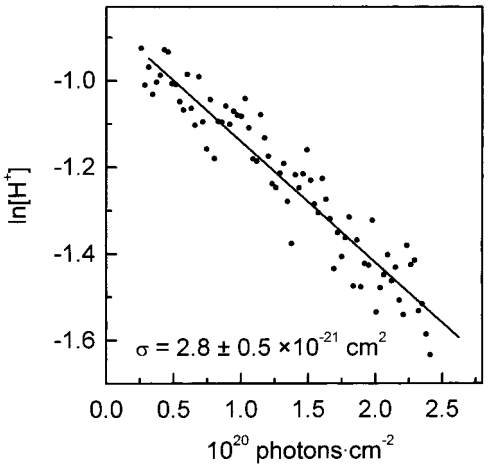

Figure 2. Semilogrithmic plot of H signal as a function of photon exposure on Si(100)−(2 × 1):H. The solid line is a least-squares linear fit, the slope of which yields the cross section. The photodesorption laser (157 nm) is unpolarized, and the angle-of-incidence is 30°. Atomic hydrogen is detected by resonance-enhanced multiphoton ionization (REMPI).

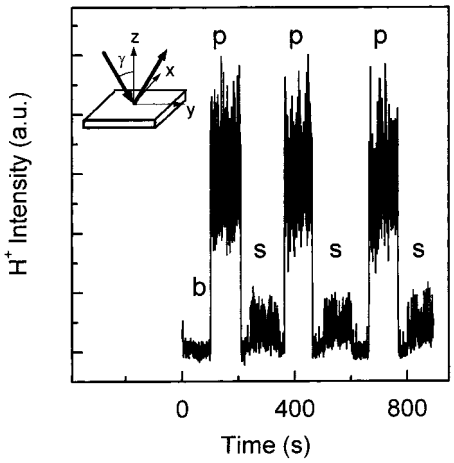

Figure 3. Photodesorption signal for s- and p-polarized 157 nm light at $\gamma = 30°$. Labels: b = baseline; p = p-polarization; s = s-polarization. The inset shows the experimental geometry. Direction of the incident light and the surface normal constitute the plane of incidence. For p-polarization, the electric field vector is in the plane of incidence, while for s-polarization, the electric field vector is perpendicular to the plane of incidence.

hydrogen, as detected by REMPI. Figure 2 shows on a semilogrithmic scale the decay of the atomic hydrogen signal as a function of accumulated exposure to 7.9 eV photons. The data (points) can be well described by a straight line, indicating first-order kinetics. Based on the slope of the least-squares linear fit (solid line), we obtain a photodesorption cross section of $\sigma_H = 2.8 \pm 0.5 \times 10^{-21}$ cm^2. Note that this cross section is obtained for unpolarized light at an angle of incidence of 30° from surface normal. The photodesorption cross section should depend on both polarization and angle of incidence, as shown below. The experimentally measured photodesorption cross section is of the same order as the cross section (4×10^{-21} cm^2) for STM-induced hydrogen desorption from Si(100) at electron energies above 6 eV.[21]

The observed photodesorption of atomic hydrogen from Si(100) cannot be due to laser-induced transient heating. With a pulse energy of 2 mJ/cm^2 and a pulse width of 25 ns, the calculated maximum temperature rise is less than 10 K, which is issufficient to induce thermal chemistry. Laser-induced thermal desorption only occurs at much higher laser pulse energies, and it should yield molecular H_2,[23] not atomic H. Note that photodesorption of atomic hydrogen from monohydride-covered Si surfaces does not occur at lower photon energies.[29] H^+ was the only observed signal in the time-of-flight mass spectrum when the monohydride-covered Si(100) surface was irradiated by 157 nm laser light. Previous studies showed substrate-mediated photodesorption of atomic Si from clean silicon surfaces,[30] but with cross sections 2 orders of magnitude lower than that for atomic hydrogen here. In the present study, we focus on the detection of atomic hydrogen during the irradiation of Si(100)−(2 × 1):H by 157 nm light. We are not able to detect any molecular hydrogen photodesorption by QMS due to the unavoidable H_2 background in a UHV system. The detection of D_2 from the Si(100)−(2 × 1):D surface is not attempted, in view of the much smaller photochemical cross section due to isotope effect. As shown below, photodesorption is due to optical excitation of the $\sigma \rightarrow \sigma^*$ transition of the H−Si bond. The force responsible for bond breaking is along the H−Si bond direction, which is close to surface normal. Thus, we expect atomic hydrogen to be the dominant photochemical product. Recently, Pusel et al. reported the observation of nonthermal desorption of H_2 when the Si(111)−H surface was irradiated by 157 nm light by electron bombardment ionization quadrupole mass spectrometry (QMS), although their signal from background H_2 in the stainless steel UHV system could account for up to 90% of the total H_2 signal.[23] The authors justified this puzzling observation by molecular dynamics simulation, which showed that only for photodesorbed atomic hydrogen with flight directions deviating strongly from the surface normal could H_2 formation become possible from reactive scattering. They estimated from this simulation that 10−20% of photodesorbed atomic H may lead to H_2 desorption. Since H_2 desorption, if present for Si(100)−(2 × 1):H, can only be a minor and secondary reaction channel, we focus on atomic hydrogen in the present study.

To unambiguously establish the initial excitation mechanism, we have measured the photodesorption yields using polarized light. The idea is straightforward, if the observed process is due to initial excitation in the substrate, the photodesorption yield should scale with substrate absorbance; if it is due to direct optical excitation, the photodesorption yield is related to the transition dipole moment and the electric field intensity, as determined by Fermi's golden rule. The inset in Figure 3 illustrates the experimental geometry. The directions of incoming light and the surface normal constitute the plane of incidence. For p-polarization, the electric field vector is in this plane; for s-polarization, the electric field vector is perpendicular to the plane of incidence. The electric field intensities ($\langle E_x^2 \rangle$, $\langle E_y^2 \rangle$, $\langle E_z^2 \rangle$) and substrate absorbances (A_p, A_s), as a function of the angle of incidence (γ), can be calculated from Fresnel's equations.[31] We use ratios between p- and s-polarization in comparing to experiment because this procedure eliminates all variations due to sample geometry and detection efficiency. For photodesorption initiated by excitation in the substrate, the ratio in photodesorption yields (Y) for p- and s-polarization is equal to the ratio of substrate absorbances,[31]

$$\frac{Y_p}{Y_s} = \frac{A_p}{A_s} \tag{1}$$

If direct optical excitation is responsible, the ratio can be obtained from Fermi's golden rule as[31]

$$\frac{Y_p}{Y_s} = \frac{0.5 \sin^2 \theta_o \langle E_x^2 \rangle + \cos^2 \theta_o \langle E_z^2 \rangle}{0.5 \sin^2 \theta_o \langle E_y^2 \rangle} \quad (2)$$

where θ_o is the angle of the transition dipole moment from the surface normal. We have taken into account the fact that the Si(100)−(2 × 1):H surface possesses C_2 rotational symmetry and there are two kinds of equally populated domains orthogonal to each other.[26]

We have carried out experimental measurements at angles of $\gamma = 0°$ and 30°. At these two angles, the position of the laser spot on the surface can be precisely determined via exit viewports. There is no background interference due to reflected light. Figure 3 illustrates a typical set of measurements for $\gamma = 30°$. Here, the atomic hydrogen signal is detected by REMPI while the polarization of the 157 nm laser is switched between s and p under otherwise identical experimental conditions. From repeated measurements, we obtained $Y_p/Y_s = 10 \pm 5$. The relatively large error bar reflects the low signal level for s-polarization. At normal incidence, Y_p/Y_s is, within experimental uncertainty, unity.

The experimentally determined ratios are compared with predictions from eqs 1 and 2 in Figure 4. At $\gamma = 0°$, the experimental ratio of Y_p/Y_s is unity, as expected for either direct or substrate excitations. At $\gamma = 30°$, the experimental ratio is much higher than A_p/A_s, which is equal to 1.3 (dashed curve). This result eliminates any mechanism due to initial excitation in the substrate. The experimental ratio in photodesorption yield can be accounted for by direct optical excitation with a transition dipole moment oriented at $\theta_o \approx 18°$ from the surface normal (solid curve). The orientation of the transition dipole moment is in excellent agreement with the H−Si bond angle. For example, an ab initio calculation[32] predicted a Si−H bond angle of $\theta_o = 19.4°$, while a molecular dynamics simulation[33] gave $\theta_o = 22°$. The dotted and dash−dotted curves show that the error range in Y_p/Y_s corresponds to a θ_o between 15° and 25°.

As discussed earlier, spectroscopic measurements and theoretical investigations identified a $\sigma \rightarrow \sigma^*$ transition for the H−Si bond on Si(100). This transition was believed to be responsible for electron-induced desorption of hydrogen in STM at electron energies above 6 eV. The energy for the $\sigma \rightarrow \sigma^*$ transition is ~8 eV, which is in resonance with the 7.9 eV photon energy from the 157 nm laser light. For optical excitation of a $\sigma \rightarrow \sigma^*$ transition, the transition dipole moment should lie along the bond direction. This is verified in our polarization measurement. All these lead us to conclude that the observed photodesorption of atomic hydrogen from Si(100)−(2 × 1):H at 157 nm results from the direct optical excitation of the $\sigma \rightarrow \sigma^*$ transition within the localized H−Si bond.

The above experiment unambiguously establishes the dissociation of a surface bond by direct optical excitation. This finding is significant because it provides an extreme example for bond-selective chemistry in large chemical systems and establishes a molecular view for optical excitation of sufficiently localized bonding on semiconductor surfaces. Such a molecular view is certainly not conventional since the adsorbate−surface bond is regarded as part of an extended surface electronic and vibrational structure. However, we must understand the limitations of such a localized picture. The strong interaction between the adsorbate−surface bond and the delocalized surface and substrate electronic structure undoubtedly results in an ultrashort lifetime for a localized electronic excitation. This is a salient feature which distinguishes direct photodesorption from photodissociation in molecular systems. In the following, we address this kind of ultrafast dynamics from both experiment and simulation.

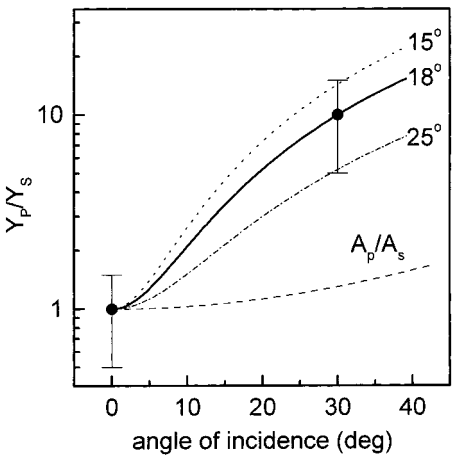

Figure 4. Comparison of measured ratio of photodesorption yields under p- and s-polarized light irradiation (two data points) with the ratios obtained from Fermi's golden rule. The curves are for transition dipole moments oriented at $\theta_o = 18°$ (solid), 15° (dotted), and 25° (dot−dashed), respectively. The ratio of substrate absorbance (A_p/A_s, dashed curve) is also shown. Optical constants of silicon: $n = 0.478$, $k = 2.00$ at $h\nu = 7.9$ eV.[44]

3.2. Time-of-Flight Distribution and Isotope Effect. We probe the dynamics of atomic hydrogen photodesorption from Si(100) in two experimental measurements: (1) translational distribution of H and (2) isotope effect in photodesorption cross section. Both are directly related to the lifetime of electronic excitation and potential energy surfaces involved. This will become apparent when we present time-dependent quantum mechanical simulation in section 3.3.

The translational energy distribution of the photodesorption product is determined in time-of-flight distribution measurement. In this experiment, the H signal is measured as a function of the delay time between probe and desorption laser pulses. The direction of the 157 nm desorption laser is normal to the surface; the focal point of the probe laser is at surface normal and 17 mm away from the 1 mm^2 irradiated spot at the center of the sample. In this geometry, the length (L) of the probe volume is relatively long. If we take L as twice the Rayleigh range, we calculated that $L = 15$ mm.[34] Thus, the time-of-flight distribution presented here is angle-integrated, covering a range of ±23° from the surface normal. If we assume that the trajectory of atomic H desorbing from the Si(100) surface is predominantly along the Si−H bond direction, i.e., ~18° from the surface normal, we estimate an error of +0.9 mm in the actual flight distance. This small error is within our experimental uncertainty and will be neglected in the following.

The data points in Figure 5 are from experimental TOF measurements. The solid line is fit to a modified Maxwell−Boltzmann distribution,[9] which yields a mean translational energy of $\langle E_{trans} \rangle = 0.24 \pm 0.02$ eV. This translational energy accounts for only a small fraction of the total available energy of $h\nu - E_D \approx 5$ eV, where E_D is the H−Si bond energy.[35] This is in contrast to simple gas-phase photodissociation reactions where atomic hydrogen is expected to carry away the majority of the total available energy. Such a low translational energy is characteristic of the ultrashort lifetime of an electronically excited state on surfaces.[8−10] We will address this issue quantitatively in time-dependent quantum mechanical simulation below.

Insight into this ultrafast dynamic process can also be obtained from the isotope effect in photodesorption yields. Within the

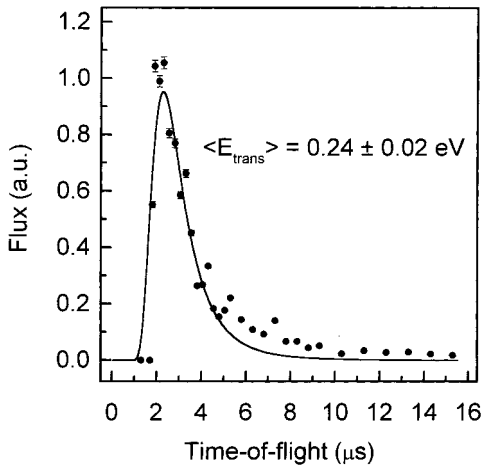

Figure 5. Time-of-flight (TOF) spectrum of atomic hydrogen photodesorbed from Si(100)−(2 × 1):H at 157 nm (normal light incidence). The flight distance is 17 mm. The solid line is fit to a modified Maxwell−Boltzmann distribution. Note that the error bar on each data point only reflects counting statistics, not including other experimental error which gives a total estimated uncertainty of approximately ±10%.

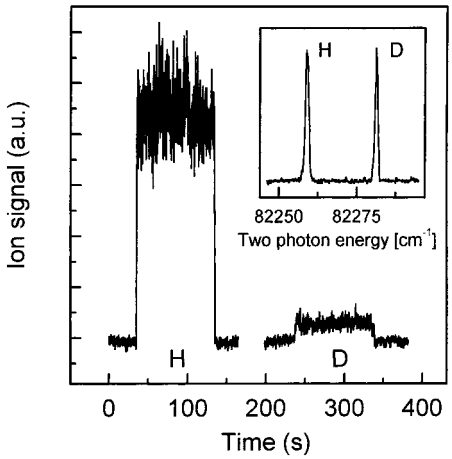

Figure 6. Photodesorption signal for H (40−140 s) and D (240−340 s) detected when a Si(100) monohydride surface with isotopically mixed but equal coverages is irradiated at normal incidence by 157 nm light. The atomic signal is detected by REMPI. The inset shows a REMPI spectrum of both H and D with equal concentration in the gas phase.

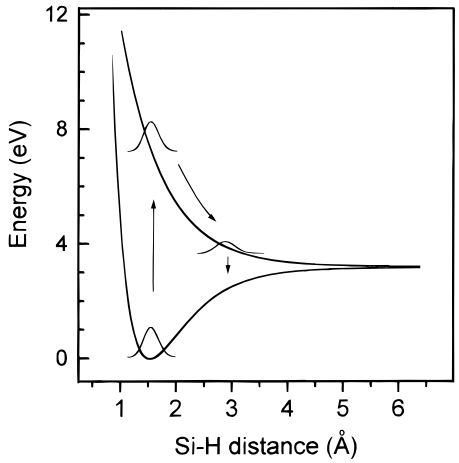

Figure 7. Ab initio potential energy surfaces for the $\sigma \rightarrow \sigma^*$ transition and snapshots of the wave function at the moments of resonant excitation and electronic quenching.

Born−Oppenheimer approximation, the Menzel−Gomer−Redhead (MGR)[36,37] model for desorption induced by electronic transitions (DIET) assumes three steps: (i) an instantaneous electronic excitation step; (ii) evolution of the system on the excited PES; (iii) an instantaneous quenching step. If the particle has gained enough kinetic energy on the excited PES during the short lifetime, it may overcome the remaining barrier on the ground PES and desorb. Such a classical model predicts an inherent isotope or mass effect. This is because a heavier particle is accelerated more slowly on the excited PES and, thus, in competition with quenching, has a lower probability to reach the critical distance for desorption. Since the difference in the electronic structure of isotope-labeled molecules is negligible in the adsorbate state, the potential energy surfaces, as well as the excitation/quenching rates, can be assumed to be isotope-independent. On the basis of Newtonian equations, it can be easily shown that the isotope effect in photodesorption cross section is given by[13]

$$\frac{y_1}{y_2} = \left(\frac{1}{Q_1}\right)^{\mu_2/\mu_1 - 1} \tag{3}$$

where y_1 and y_2 are the photodesorption yields for the isotope-labeled leaving particles with reduced masses μ_1 and μ_2, respectively. Q_1 is the quantum yield for the desorption of particle 1.

In the experiment, we prepare an isotopically mixed Si(100) monohydride surface by exposing the surface to a mixture of H and D with nearly equal concentration. A REMPI spectrum of the gas mixture is shown in the inset of Figure 6. The H and D ion signals are of equal intensity in this spectrum. Thermal desorption spectroscopy (TDS) from the mixed surface reveals that the coverages of H and D on the surface are, within ±10%, equal to each other (data not shown). These measurements indicate that the atomic adsorption probabilities as well as the REMPI detection efficiencies are the same for both H and D.

The mixed Si(100)−(2 × 1):H,D surface is irradiated at normal incidence by the 157 nm desorption laser, while the probe laser wavelength is switched between the two peak positions for H and D detection. A typical set of measurements is shown in Figure 6. From repeated measurements, we obtain an isotope ratio in photodesorption yield of $y_H/y_D = 10 \pm 3$. Based on eq 3, we obtain a quantum yield of 0.09 for atomic H. This quantum yield is more than 10^3 times the value obtained in quantum mechanical simulation shown below and demonstrates the complete failure of Newtonian mechanics in describing an inherently quantum mechanical problem.

Note that in STM studies of electron-induced desorption of hydrogen from the same surface, Avouris et al. estimated an isotope ratio of $y_H/y_D \approx 50$ for the electronic mechanism at bias voltages greater than 6 eV.[38] In principle, the electronic mechanism in STM studies should involve the same $\sigma \rightarrow \sigma^*$ transition. We do not understand the difference in isotope ratio between our measurement and the STM study. One possible explanation is that the strong electric field present locally in STM may have an effect on both excitation and quenching rates. This issue may deserve further investigation.

3.3. Time-Dependent Quantum Mechanical Simulation. To understand the dynamics of the direct photodesorption process, we have carried out time-dependent quantum mechanical simulation within the spirit of the MGR model, i.e., Born−Oppenheimer approximations. This is shown schematically in Figure 7 using ab initio potential energy surfaces[38] for the $\sigma \rightarrow \sigma^*$ transition and snapshots of the wave function at the moments of resonant excitation and electronic quenching. The simulation involves numerical solution of the time-dependent Schrodinger

equation for the nuclear wave function (in atomic units)

$$i\frac{\partial\psi(z,t)}{\partial t} = \hat{H}\psi(z,t) \tag{4}$$

where z is the H−Si distance. The initial wave function, $\psi(z,0)$, is the ground vibrational eigenfunction on the ground PES. The Hamiltonian is switched at $t = 0$ from that for the ground PES ($\hat{H}_g$) to that of the excited PES ($\hat{H}_e$). This is the initial electronic excitation step. After propagation on the excited PES for a residence lifetime τ_R, the Hamiltonian is switched back to ($\hat{H}_g$) to represent electronic quenching. The wave function further propagates on the ground PES for $t > \tau_R$, and part of it may reach the asymptotic limit for desorption.

The ground- (U_g) and excited-state (U_e) potential energy surfaces are from ab initio calculations of Avouris et al. on hydrogenated silicon clusters.[38] The ab initio results can be represented by a Morse potential for U_g and an exponential function for U_e,

$$U_g(z) = D[1 - e^{-b(z-z_o)}]^2 \tag{5}$$

$$U_e(z) = D' e^{-b'(z-z_o')} \tag{6}$$

where $D = 0.117$ au, $b = 0.812$ au^{-1}, $z_o = 2.872$ au, $D' = 0.0368$ au, $b' = 0.710$ au^{-1}, and $z_o' = 4.877$ au.

All simulations are carried out at a temperature of 0 K. We have also carried out simulation for higher temperatures by including excited vibrational states on U_g in the initial wave function but find the simulated desorption yield and translational energy distribution are nearly independent of temperature for $T < 450$ K.

We carry out simulation in discrete phase space using the fast Fourier transform method for propagation.[39] The spatial grid size is 4096 points; the z range is from 0.5 to 200 atomic units (au), with grid spacing of 0.0487 au. This large z range is chosen to avoid any possible error introduced at the boundaries. This is necessary particularly for very low desorption yields at short τ_R. The time step used in propagation is 10^{-3} fs. The total propagation time is $t_m = 12\,400$ au (300 fs) for H and $t_m = 20\,670$ au (500 fs) for D. At the end of each propagation, the total wave function is separated into a bound part and a desorbed part. The latter is defined as

$$\psi_a(z,t,\tau_R) = f(z,z_d)\,\psi(z,t,\tau_R) \tag{7}$$

where $f(z)$ is a Fermi-type cutoff function to smoothly separate the desorbed from the trapped wave packet.[40] The cutoff distance, z_d, is chosen to be 12 au. The desorption yield is the norm, $\langle|\psi_a|^2\rangle$, of the asymptotic wave function in eq 7 for $t = t_m$. Figure 8 shows $\langle|\psi_a|^2\rangle$ as a function of propagation time for several excited-state residence times. The long propagation time of $t_m = 300$ fs is needed to guarantee that the obtained desorption yield corresponds to the saturation value of $\langle|\psi_a|^2\rangle$. The use of shorter propagation time may systematically underestimate the desorption yield, particularly for shorter τ_R. Figure 9 shows the simulated desorption probability, $p(\tau_R)$, as a function of τ_R for both H and D. Classically, there is a critical residence time, τ_c, above which desorption occurs (dashed lines). As expected, the classical times are at the inflection points of quantum mechanical results for both H and D.

In the absence of quantitative treatment of the electronic quenching mechanism, we may assume that the quenching rate is coordinate-independent and can be represented by a constant lifetime, τ, which accounts for a continuous and exponential

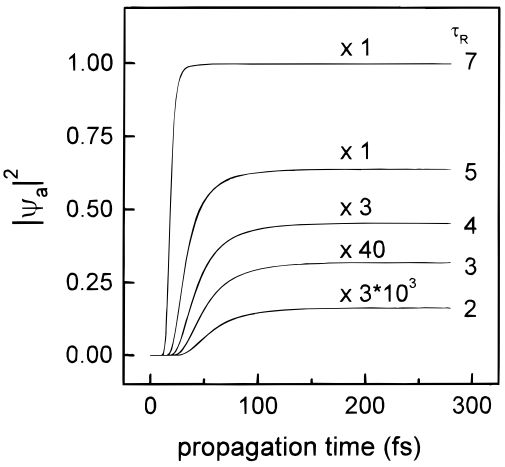

Figure 8. The norm of the desorbed wave packet as a function of total propagation time on the ground PES for indicated residence times on the excited PES. Note the scaling factor for each curve.

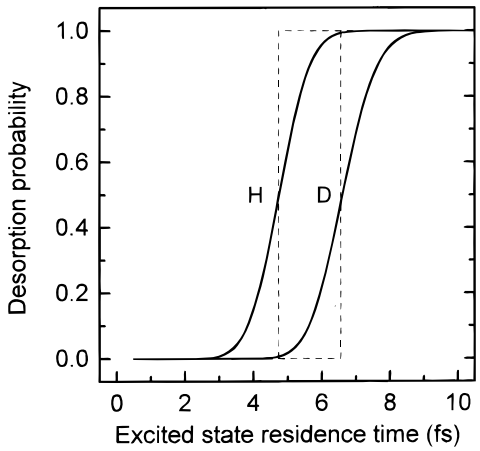

Figure 9. Calculated desorption yields for both H and D as a function of excited-state residence time, τ_R, from quantum mechanical simulation (solid curves) and classical mechanics (dashed lines).

decay from the excited state. The dependence of the desorption quantum yield Q on the true lifetime, τ, can be obtained from an incoherent averaging of quantum trajectories,

$$Q(\tau) = \frac{\sum_{i=1}^{N} p(\tau_{Ri}) \exp\left(-\frac{\tau_{Ri}}{\tau}\right)}{\sum_{i=1}^{N} \exp\left(-\frac{\tau_{Ri}}{\tau}\right)} \tag{8}$$

where i is the index for the quantum trajectories with residence time of τ_{Ri}. We have carried out simulations for $\tau_R = 0-10$ fs, with 0.1 fs steps ($N = 100$). Figure 10 shows the lifetime-averaged desorption quantum yields (Q_H, Q_D, left axis) for both H (long dashed curve) and D (short-dashed curve), as well as the isotope ratio Q_H/Q_D (solid curve, right axis). While both Q_H and Q_D increase with τ, the isotope ratio Q_H/Q_D decreases with increasing τ and approaches unity for $\tau > 10$ fs. The experimentally measured isotope ratio of $Q_H/Q_D = 10$ corresponds to an excited-state lifetime of $\tau = 0.4$ fs and a quantum yield (for H) of $Q_H = 2 \times 10^{-5}$. Note that, for a lifetime of $\tau = 0.4$ fs, the most important contribution to the total desorption yield in eq 8 comes from $\tau_R \approx 4$ fs, as shown in the inset of Figure 10.

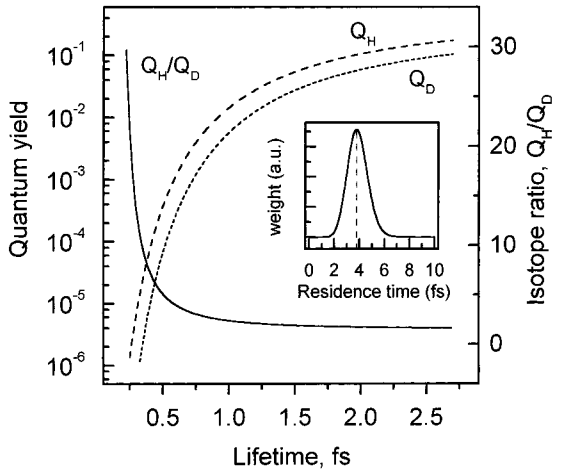

Figure 10. Calculated desorption quantum yields (left axis) for both H (Q_H, long dashed curve) and D (Q_D, short-dashed curve) and the isotope ratio in photodesorption quantum yield (Q_H/Q_D, right axis) as a function of excited-state lifetime, τ. The experimental isotope ratio corresponds to an excited-state lifetime of ~0.4 fs. The inset shows the contribution to the total desorption yield {weight = $p(\tau_R)$ exp($-\tau_R/\tau$), where τ = 0.4 fs} as a function of excited-state residence time, τ_R.

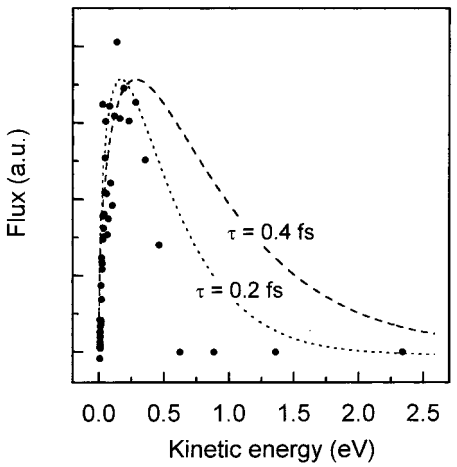

Figure 11. Comparison of translational energy distributions for atomic hydrogen obtained from experimental TOF spectrum in Figure 5 (dots) and time-dependent quantum mechanical simulations (dashed curve) for excited-state lifetimes of τ = 0.2 and 0.4 fs, respectively.

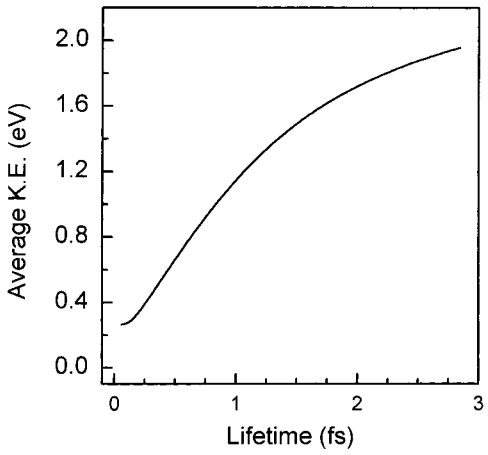

Figure 12. Flux-weighted mean translational energy for H as a function of excited-state lifetime τ obtained from time-dependent quantum mechanical simulation.

The quantum yield calculated from classical mechanics in eq 3 is more than 3 orders of magnitude higher than that obtained from quantum mechanical simulation. We believe classical mechanics is inadequate in treating DIET processes with ultrashort lifetimes and, thus, very low quantum yields. This is particularly true for low masses. One must be cautious in attempting to understand an inherently quantum mechanical problem, such as the photodesorption of atomic H from Si(100), using classical or semiclassical models.

In addition to quantum yields, the translational distribution of photodesorbed H can also be easily obtained from the simulation. This is simply done by Fourier transform of the desorbed wave packet to give $\psi_a(p)$ in momentum (p) space. The translational energy distribution in the density domain is $|\psi_a(p)|^2$ dp/dE vs E, where the factor dp/dE ($\propto 1/p$) is the Jacobian for the transformation from momentum to energy space. A further transformation from density to flux domain requires the multiplication by velocity ($\propto p$). Thus, the two factors from these transformations cancel out and $|\psi_a(p)|^2$ vs E is the translational energy distribution in the flux domain. Finally, we use a lifetime averaging procedure similar to eq 8 to obtain the translational distribution for a particular lifetime, τ. Figure 11 shows the simulated translational energy distributions of atomic H for two excited-state lifetimes, τ = 0.2 and 0.4 fs, respectively. For comparison, the dots are experimental data obtained from the TOF distribution in Figure 5. All spectra have been normalized to give the same peak intensity. The simulated translational distribution for τ = 0.4 fs extends to significantly higher kinetic energies than that of the experimental spectrum. Even for τ = 0.2 fs, while the peak kinetic energy agrees with that of the experimental distribution, the simulated distribution is broader. The flux-weighted mean translational energies from simulations are 0.56 and 0.34 eV for τ = 0.4 and 0.2 fs, respectively, as compared to the experimental value of 0.24 eV. Figure 12 shows the flux-weighted mean translational energy, $\langle E_{trans}\rangle$, obtained from simulation as a function of excited-state lifetime, τ. $\langle E_{trans}\rangle$ increases with τ and, when $\tau \rightarrow \infty$, approaches the value of 4.7 eV, which is the total available energy from the photodissociation of the H−Si bond.

We may identity a number of reasons for the disagreement in translational energy distributions between experiment and simulation. The above simulation neglects possible energy loss on the ground PES on which desorption completes within 10^2 fs. Unlike vibrational excitation deep in the adsorption well where relaxation to phonons is inefficient due to energy mismatch,[7] the nearly continuous energy near the top of the potential well may be partially lost to surface and substrate vibrations within this short time window. Another limitation is the one-dimensionality of the model employed. A more accurate treatment should use two or three dimensions to take into account H−Si bending vibrations on the surface. Finally, the applicability of the Born−Oppenheimer approximation may be questionable when we address an ultrafast dynamic process with a femtosecond or subfemtosecond lifetime. A more realistic simulation should treat electronic and nuclear degrees of freedom simultaneously. This is certainly a difficult task. All these issues deserve further investigation.

In passing, we note that similar simulations have been carried out recently by Boendgen and Saalfrank for the STM-induced desorption of hydrogen from silicon surfaces using both time-dependent wave packet and density matrix methods.[41] Results from their wave packet simulation are qualitatively similar to those presented above. However, we also notice some quantitative differences, particularly in the calculated quantum yields

and isotope ratios. For the same lifetime, their simulation gave somewhat lower quantum yields and, therefore, a higher isotope ratio. This discrepancy could be due to differences in quantitative details of simulation parameters. For example, they used a smaller grid, a longer time step, and a shorter propagation time than those employed in our simulation. All these may result in lower quantum yields in their simulation.

3.4. Applications in Semiconductor Technology. The direct photodissociation of the H−Si bond on silicon surfaces may find applications in resistless photolithography. The creation of reactive surface sites by direct photodesorption may be used for further selective growth or reaction, such as local oxidation. An obvious advantage is that growth and patterning of surface structures can be carried out in situ. This scheme has been demonstrated successfully in previous STM writing experiments.[42,43] STM writing is a serial process and is inherently limited to slow processing speed, while patterning by lasers is a parallel process. There are a number of mechanisms in laser-induced surface patterning, including gas-phase photodissociation, laser-induced local heating, hot carrier mediated photoexcitations, and direct photodissociation on surfaces. Spatial resolution in the gas-phase photodissociation mechanism is limited by mass transport, while the local heating and the hot carrier mechanisms are limited by the scales of thermal and carrier diffusion, respectively. On the other hand, spatial resolution in patterning by direct surface photodissociation is only limited by light diffraction. Therefore, the direct surface photodissociation mechanism can provide the best spatial resolution in laser surface patterning. We must point out that the application of 157 nm photodesorption of H from silicon surfaces to resistless lithography may be limited by the low cross section and quantum yield. This difficulty may be overcome with the development of more powerful VUV lasers.

4. Conclusions

(1) Irradiation of the Si(100)−(2 × 1):H monohydride surface by 157 nm laser light leads to the desorption of atomic hydrogen, with a cross section of $\sim 3 \times 10^{-21}$ cm^2. The photodesorbed atomic hydrogen is characterized by a mean translational energy of $\langle E_{trans} \rangle = 0.24 \pm 0.02$ eV and an isotope effect in photodesorption yield of $y_H/y_D = 10 \pm 3$.

(2) Measurement using polarized light shows that the transition dipole moment for the optical excitation is oriented at ∼18° from surface normal, in agreement with the H−Si bond direction. This result establishes the dissociation of the H−Si bond by direct optical excitation of the $\sigma \rightarrow \sigma^*$ transition.

(3) Time-dependent quantum mechanical simulation on the ab initio potential energy surfaces suggests that the experimental isotope effect corresponds to an excited-state lifetime of ∼0.4 fs and a quantum yield for atomic hydrogen desorption of $Q_H \approx 10^{-5}$. However, the simulated mean translational energy obtained for atomic H is 2−3 times the experimental value. This disagreement may be attributed to the neglect of energy loss on the ground PES and/or to the limitations of the one-dimensional model and the Born−Oppenheimer approximation.

Acknowledgment. This work was supported by the National Science Foundation, Research Corporation, the University of Minnesota, and the Minnesota Supercomputer Institute. One of us (X.Y.Z.) thanks J. Manz for introducing him to wave packet dynamics. We thank Phaedon Avouris for providing ab initio results.

References and Notes

(1) Lin, J.-T.; George, T. F. *J. Chem. Phys.* **1980**, *72*, 2554.
(2) Jedrzejek, C.; Freed, K. F.; Efrima, S.; Metiu, H. *Surf. Sci.* **1981**, *109*, 191.
(3) Chuang, T. J. *Surf. Sci. Rep.* **1983**, *3*, 1.
(4) Heidberg, J.; Stein, H.; Weiss, H. *Surf. Sci.*, **1987**, *184*, L431.
(5) Chang, H.-C., Ewing, G. E. *Chem. Phys.*, **1989**, *139*, 55.
(6) Hassel, M.; Svensson, K.; Persson, M.; Andersson, S. *Phys. Rev. Lett.* **1998**, *80*, 2481.
(7) Cavanagh, R. R.; King, D. S.; Stephenson, J. C.; Heinz, T. F. *J. Phys. Chem.* **1993**, *97*, 786 references therein.
(8) Avouris, Ph.; Walkup, R. E. *Annu. Rev. Phys. Chem.* **1989**, *45*, 173.
(9) Zhu, X.-Y. *Annu. Rev. Phys. Chem.* **1994**, *45*, 113.
(10) Zimmermann, F. M.; Ho, W. *Surf. Sci. Rep.* **1995**, *22*, 127.
(11) Zhu, X.-Y.; White, J. M. *Phys. Rev. Lett.* **1992**, *68*, 3359.
(12) Zhu, X.-Y.; Wolf, M.; Huett, T.; White, J. M. *J. Chem. Phys.* **1992**, *97*, 5868.
(13) Zhu, X.-Y. *Mod. Phys. Lett. B* **1992**, *6*, 1893.
(14) Wolf, M.; Hertel, T.; Ertl, G. *J. Chem. Phys.* **1995**, *102*, 3414.
(15) Burns, A. R.; Stechel, E. B.; Jennison, D. R.; Li, Y. S. *Phys. Rev. Lett.* **1994**, *72*, 3895.
(16) Liu, L.; Guo, H.; Seideman, T. *J. Chem. Phys.* **1996**, *104*, 8757.
(17) Bornscheuer, K. H.; Nessler, W.; Binetti, M.; Hasselbrink, E.; Saalfrank, P. *Phys. Rev. Lett.* **1997**, *78*, 1174.
(18) Watanabe, K.; Sawabe, K.; Matsumoto, Y. *Phys. Rev. Lett.* **1996**, *76*, 1751.
(19) Maruno, S.; Iwasaki, H.; Horioka, K.; Li, S.-T.; Nakamura, S. *Phys. Rev. B* **1983**, *27*, 4110.
(20) Ciraci, S.; Butz, R.; Oellig, E. M.; Wagner, H. *Phys. Rev. B* **1984**, *30*, 711.
(21) Shen, T.-C.; Wanf, C.; Abeln, G. C.; Tucker, J. R.; Lyding, J. W.; Avouris, Ph.; Walkup, R. E. *Science* **1995**, *268*, 1590.
(22) Akazawa, H.; Utsumi, Y. *J. Appl. Phys.* **1995**, *78*, 2725.
(23) Pusel, A.; Wetterauer, U.; Hess, P. *Phys. Rev. Lett.* **1998**, *81*, 645.
(24) Vondrak, T.; Zhu, X.-Y. *Phys. Rev. Lett*, **1999**, *82*, 1967.
(25) Nishino, H.; Yang, W.; Dohnalek, Z.; Ukraintsev, V.; Yates, J. T., Jr. *J. Vac. Sci. Technol.* **1997**, *A15*, 182.
(26) Boland, J. J. *Surf. Sci.* **1992**, *261*, 17.
(27) Waltenburg, H. N.; Yates, J. T., Jr. *Chem. Rev.* **1995**, *95*, 1589.
(28) Hansch, T. W.; Lee, S. A.; Wallenstein, R.; Wieman, C. *Phys. Rev. Lett.* **1975**, *34*, 307.
(29) Komori, F.; Shudo, K.; Hattori, K.; Iimori, T.; Murata, Y. *Surf. Sci.* **1996**, *363*, 268.
(30) Chen, X. H.; Polanyi, J. C.; Rogers, D. *Surf. Sci.* **1997**, *376*, 77.
(31) Zhu, X.-Y.; White, J. M.; Wolf, M.; Hasselbrink, E.; Ertl, G. *Chem. Phys. Lett.* **1991**, *176*, 459.
(32) Jing, Z.; Whitten, J. L. *Phys. Rev. B* **1992**, *46*, 9544.
(33) Kohen, D.; Tully, J. C.; Stillinger, F. H. *Surf. Sci.* **1998**, *397*, 225.
(34) The Rayleigh range is the distance at which the laser beam expands to $\sqrt{2}$ times the beam waist. Assuming a diffraction-limited laser beam, $L = (2\pi w_o^2)/\lambda$, where λ is the laser wavelength; w_o, the beam waist, is given by $2f\lambda/D$, where f is the focal length of the lens and D is the diameter of the beam ($\lambda = 243$ nm; $f = 25$ cm; $D = 5$ mm).
(35) Doren, D. *Adv. Chem. Phys.* **1996**, *95*, 1.
(36) Menzel, D.; Gomer, R. *J. Chem. Phys.* **1964**, *41*, 3311.
(37) Redhead, P. A. *Can. J. Phys.* **1964**, *42*, 886.
(38) Avouris, Ph.; Walkup, R. E.; Rossi, A. R.; Shen, T. C.; Abeln, G. C.; Tucker, J. R.; Lyding, J. W. *Chem. Phys. Lett.* **1996**, *257*, 148.
(39) Kosloff, D.; Kosloff, R. *J. Comput. Phys.* **1983**, *52*, 35.
(40) Heather, R.; Metiu, H. *J. Chem. Phys.* **1987**, *86*, 5009.
(41) Boendgen, G.; Saalfrank, P. *J. Phys. Chem.* **1998**, *102*, 8029.
(42) Snow, E. S.; Campbell, P. M.; McMarr, P. J. *Appl. Phys. Lett.* **1993**, *63*, 749.
(43) Lyding, J. W.; Shen, T.-C.; Hubacek, J. S.; Tucker, J. R.; Abeln, G. C. *Appl. Phys. Lett.* **1994**, *64*, 2010.
(44) *CRC Handbook of Chemistry and Physics*, 79th ed.; Lide, D. R., Ed.; CRC Press: Boca Raton, 1998.